[redacted]

Copy 7
RM L56I28

C.3

NACA RM L56I28

UNCLASSIFIED

NACA

RESEARCH MEMORANDUM

FLUTTER CHARACTERISTICS AT TRANSONIC SPEEDS OF A 45° SWEPTBACK WING WITH AND WITHOUT INBOARD MODIFICATIONS AT THE LEADING AND TRAILING EDGES

By Thomas B. Sellers and Norman S. Land

Langley Aeronautical Laboratory
Langley Field, Va.

NATIONAL ADVISORY COMMITTEE
FOR AERONAUTICS

WASHINGTON

January 9, 1957

[redacted]

UNCLASSIFIED

ERRATA

NACA Research Memorandum L56I28

By Thomas B. Sellers and Norman S. Land
January 1957

Page 11: The values of a and r_α^2 in columns 3 and 4 of table I for model 1a should be interchanged; the values under the heading a should be listed under the heading r_α^2 and vice versa. The values for model 2a are correct as given.

Issued 4-3-57

NACA RM L56I28

NATIONAL ADVISORY COMMITTEE FOR AERONAUTICS

RESEARCH MEMORANDUM

FLUTTER CHARACTERISTICS AT TRANSONIC SPEEDS OF A 45° SWEPTBACK WING WITH AND WITHOUT INBOARD MODIFICATIONS AT THE LEADING AND TRAILING EDGES

By Thomas B. Sellers and Norman S. Land

SUMMARY

Flutter characteristics at transonic speeds of a model of a fighter-type-airplane wing are presented over a range of Mach numbers from 0.7 to 1.4. The airplane wing was a modification of a basic wing configuration which had the quarter-chord line swept back 45°, an aspect ratio of 3.0, a taper ratio of 0.34, and NACA 64A004 airfoil sections parallel to the plane of symmetry. The modified configuration had a change in the leading- and trailing-edge sweep at the 0.49-semispan station. The inboard section had the leading and trailing edges swept back 55° and 21°, respectively, as compared with 50° and 27° over the outboard section.

The results of the investigation indicated a rather abrupt increase in flutter-speed ratio (ratio of experimental to calculated incompressible flutter speed) near a Mach number of 1.0, after which the flutter-speed ratio changed only slightly as the Mach number was increased to 1.4. Flutter characteristics of the basic wing configuration were similar to those of the modified configuration.

INTRODUCTION

The effects of wing plan form on flutter in the transonic speed range have been the subject of a number of recent investigations. The present investigation was made to determine the transonic flutter characteristics of a fighter-type-airplane wing with a somewhat different plan form from any of those previously studied in the Langley transonic blowdown tunnel (for example, ref. 1). The wing configuration was a modification of a basic wing plan form which had the quarter-chord line swept back 45°, a taper ratio of 0.34, an aspect ratio of 3.0, and

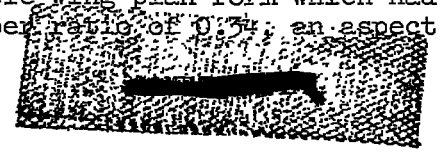

modified NACA 65A004 airfoil sections parallel to the plane of symmetry. For the modified configuration the inboard sections of the basic plan form were altered by extending the local wing chords inboard of the 49-percent-semispan station. Over the inboard region the leading and trailing edges were swept back 55° and 21°, respectively, as compared with 50° and 27° over the outboard section. The flutter boundaries of the basic wing plan form and the modified configuration were defined over a range of Mach numbers from 0.7 to 1.4 at zero lift.

SYMBOLS

A	aspect ratio including body intercept
a	distance in wing half-chords from midchord to elastic-axis position, measured positive rearward of midchord
b	half-chord perpendicular to quarter-chord line, ft
b_r	half-chord perpendicular to quarter-chord line at intersection of quarter-chord line and fuselage, ft
EI	wing bending stiffness, lb-in.^{2}
GJ	wing torsional stiffness, lb-in.^{2}
I_α	mass moment of inertia of wing about elastic axis per unit length of quarter-chord line, slug-ft^2/ft
k	reduced-frequency parameter, $\omega b/V_n$
l	length of wing along quarter-chord line from intersection of quarter-chord line with edge of fuselage to intersection of theoretical tip, ft
M	Mach number
m	mass of wing per unit length along quarter-chord line, slugs/ft
q	dynamic pressure, lb/sq in.
r_α	nondimensional radius of gyration of wing about elastic axis, $\left(I_\alpha/mb^2\right)^{1/2}$
V	stream velocity, ft/sec

[redacted]

V_e/V_R flutter-speed ratio

x_α distance in semichords (measured perpendicular to quarter-chord line) from wing elastic axis to wing center of gravity, positive when center of gravity is behind the elastic axis

η nondimensional coordinate along quarter-chord line, fraction of length l from wing-body juncture

μ ratio of mass of wing to mass of cylinder of air of diameter equal to chord of wing, both taken for equal length along quarter-chord line, $m/\pi\rho b^2$

ρ air density, slugs/cu ft

ω angular frequency of vibration, radians/sec

Subscripts:

α uncoupled torsion mode

e experimental values at start of flutter

R calculated values

n normal to quarter-chord line

MODELS

The plan forms and dimensions of the wings tested are presented in figure 1. The model with the basic wing plan form (which will be referred to as model 2a) had a quarter-chord sweepback of 45°, an aspect ratio (including the intercepted body area) of 3.0, a taper ratio of 0.34, a dihedral angle of -2.5°, and NACA 64A004 airfoil sections parallel to the plane of symmetry. Models 1a and 1b were essentially identical and differed from model 2a in that inboard of the 0.49-semispan station the local wing chords were increased. This modification of the inboard sections increased the leading-edge sweep angle from 50° to 55° and decreased the trailing-edge sweep angle from 27° to 21°. Refaired airfoil sections were employed in this region with the maximum thicknesses the same for the basic and modified sections. This resulted in decreased ratios of thickness to chord over the modified region. The models simulated an airplane wing in external geometry but were not dynamically scaled.

[redacted]

The three models tested were constructed of laminated, spanwise, mahogany strips. These strips were approximately 1/8 inch wide with the wood grain and laminations parallel to the quarter-chord line. Wire strain gages which responded to bending and torsional wing deflections were mounted on the wing surface near the root of each wing. The gage installation increased the ratio of wing thickness to chord by approximately $1\frac{1}{2}$ percent and affected approximately 42 percent of the panel span.

APPARATUS

Tunnel and Model Support System

The tests were conducted in the Langley transonic blowdown tunnel which has been shown by comparative tests in free air to yield accurate flutter data at transonic speeds (ref. 2). The operating characteristics which make this tunnel particularly suitable to flutter testing are described in reference 1. In brief, the tunnel dynamic pressure may be increased through a large range while the test-section Mach number remains constant.

A schematic drawing of the model support system is shown in figure 2. The models were rigidly mounted in a 3-inch-diameter cylindrical sting fuselage. The sting fuselage extended upstream into the subsonic flow region of the tunnel entrance cone, and the downstream end was supported by the angle-of-attack mechanism.

The extension of the sting fuselage into the subsonic region of the tunnel prevents the formation of a bow wave and its possible reflection on the model. The turbulent boundary-layer growth along the rather long sting fuselage has been calculated and gives a displacement thickness of 0.1 to 0.2 inch at the position of the model. Since the aerodynamic loading at the fixed root does not play an important part in the flutter condition, the presence of a displacement boundary-layer thickness of 0.1 to 0.2 inch, as compared with an exposed semispan of 6.3 inches, is thought to have no significant effect on the results obtained.

The degree of root fixity afforded by the sting fuselage can be judged by a comparision of the weight, frequency, and internal damping for the sting with similar quantities for the model. The sting fuselage weighs approximately 300 pounds, has a first bending frequency of 15 cycles per second, and internal damping of about 10 percent of critical. Correspondingly, the model weighs 0.2 pound, has a flutter frequency of the order of 270 cycles per second. and internal damping of about 1.0 percent of critical. A few simple response calculations will show negligible response of the sting, not only in the first bending mode, but in any higher mode for which the sting frequency might approximate the flutter frequency.

That the degree of root fixity is indeed high has been shown in flutter tests of a comparable model, in which accelerometer measurements were made of the sting response. These measurements showed no correlation between the motions of the fuselage and the model during flutter.

Instrumentation

Each wing panel was equipped with two sets of wire strain gages which were oriented on the wing so that the gages were sensitive to wing torsional and bending deflections, respectively. The outputs from these gages were fed into a multichannel automatic recording oscillograph which recorded the time histories of the bending and torsional oscillations. In addition, the tunnel stagnation temperature and pressure and the test-section static pressure were simultaneously recorded by the oscillograph.

A flutter indicating system was used during the test to detect the onset of flutter. The system consisted of two oscilloscopes, one for each wing panel. The outputs from the bending and torsion gages for each panel were fed into the horizontal and vertical axes, respectively, of one oscilloscope. Before the wing fluttered, the trace on the oscilloscope was random but, when the bending and torsion frequencies were the same (flutter), the trace formed a simple Lissajous figure.

METHODS AND TESTS

Physical Properties of Models

The values of torsional and bending stiffness of the various models were determined by the method described in reference 1. Briefly, the system was an optical one through which the bending and torsional deflections of the wings were magnified and measured when a known bending or torsional moment was applied to the wing. Usually the elastic axis is determined by clamping the wing normal to the quarter-chord line at the wing root (ref. 1) but, because of the low aspect ratio and taper ratio of the present configuration, the wing span over which the elastic axis was determined by the accepted method was small and the elastic axis was not considered applicable. Because of this limitation, the elastic axis was assumed to coincide with the torsional node line. This assumption is supported by previous experience with models of similar plan form and construction with small coupling for which the elastic axis was approximated by the torsional node line.

The spanwise distribution of the wing mass, center-of-gravity location, and the moment of inertia about the panel elastic axis were determined in the following manner. The wings were cut into 13 chordwise segments (perpendicular to the quarter-chord line) approximately 1/2 inch wide. Each segment was weighed and its center of gravity located. The moment of inertia about the elastic axis was found by swinging each segment on a torsional pendulum. Inasmuch as the root block was made of the same material as the wing panels, it was possible to obtain a more accurate representation of the mass properties of the inboard sections for use in the calculations by shaping the root block to conform with the extended wing plan form and airfoil sections. The most inboard segment was located at approximately the 0.10η station, and all the mass properties inboard of this station are extrapolated values and are marked as such in table I.

The center-of-gravity and elastic-axis locations, radius of gyration, mass per unit length, local chord ratio, and bending (EI) and torsional (GJ) stiffnesses for several spanwise stations are tabulated in table I for all three models. The mass-property differences between models 1a and 1b were assumed to be small and only one set of mass properties for that plan form is presented.

The bending and torsional frequencies that correspond to the natural cantilever modes of vibration were determined by sprinkling salt on the wing and exciting the wing over a range of frequencies with an electromagnetic vibrator. As the natural frequencies were approached, node lines were formed by the grains of stationary salt. The frequency corresponding to the most clearly defined node line was chosen as the natural frequency. The node lines and frequencies for the three models are presented in figure 3. It should be noted, from the data of figure 3, that the left-panel torsional frequencies for the three models tested were consistently lower than the corresponding frequencies for the right panel. These differences may be attributed to manufacturing techniques. In the vibration tests care was taken to duplicate the root clamping condition of the model mounting in the tunnel fuselage block.

The structural damping in bending g was measured by obtaining the logarithmic decrement from the time history of the decay of free-bending oscillations of the model. For all models the structural damping in bending was approximately 0.012.

Flutter Tests

The tests were made with the model mounted along the tunnel center line. Several low-speed runs were made and the model angle of attack was adjusted until there was no appreciable deflection of the wing tips. This angle was assumed to be the angle of zero lift.

[redacted]

At the beginning of a typical flutter test the oscillograph was started and the tunnel stagnation pressure was increased until the model was seen to flutter or the Lissajous figure was obtained on either one or both of the oscilloscopes. When flutter was apparent, the tunnel speed was reduced immediately. After each run the model was checked visually for damage. Also, the tip of the wing was deflected and released and the resulting decay of free-bending oscillations was recorded on the oscillograph. Any structural damage suffered by the wing in the previous run was shown by these records.

COMPUTATIONS

The use of a calculated reference flutter speed V_R and frequency ω_R as a basis for comparing flutter data has been outlined and described in references 1 and 3. Reference flutter speeds V_R for the three models in this series of tests have been calculated by the method used in reference 1. This method employs two-dimensional, incompressible aerodynamic coefficients in a Rayleigh type of analysis in which the flutter mode is approximated by the superposition of uncoupled free-vibration modes of a uniform cantilever beam. The aerodynamic coefficients are based on the free-stream velocity component normal to the quarter-chord line. The effect of wing taper was brought into the aerodynamic terms by allowing the reduced-frequency parameter k to vary according to the chord variation and by representing the Theodorsen functions $F(k)$ and $G(k)$ by a linear variation between their root and tip values.

Three uncoupled mode shapes which corresponded to the first bending, first torsion, and second bending modes of a uniform cantilever beam were used in the calculations. Frequencies used in the calculations were coupled and were measured as described previously. Although these frequencies corresponded to coupled modes of vibration, previous tests indicate that for similar models the coupling is small.

Values of the flutter-speed parameter $V_R/b_r\omega_\alpha$ were obtained from the solution of the flutter determinant as a function of the structural damping for given values of the air density. The assumption was made in the calculations that the structural damping in bending was equal to that in torsion and was independent of frequency. Values of the reference flutter speed V_R were then obtained by using the measured structural damping in bending for each wing, together with the appropriate air density.

[redacted]

RESULTS AND DISCUSSION

General Comments

Before discussing any specific set of flutter data it should be pointed out that, for all configurations tested at subsonic and supersonic speeds, intermittent flutter or low damping occurred over large ranges of tunnel velocity and dynamic pressure before the steady flutter point was reached. The change from intermittent to steady flutter was progressive in that the bursts of flutter became longer in time and more frequent as the tunnel velocity and dynamic pressure were increased until finally steady flutter was obtained. Because of this low damping characteristic the selection of the flutter point was somewhat arbitrary. The point at which the frequency of the bending and torsion oscillations first reached a common value, even though there were interspersed large regions of random oscillations, was selected as the start of low damping. The steady flutter point was selected as the point at which the bending and torsion frequency first came to the same value and remained equal, independent of time and increases in tunnel velocity and dynamic pressure.

In figure 4 the intermittent flutter region is indicated by the shaded area below the steady flutter boundary. The flutter boundary in figure 4 is defined in terms of q_e plotted against M_e. The data indicate that the intermittent flutter region (preceding steady flutter) extended throughout the entire Mach number range of the tests.

As shown in figure 3 the torsional frequencies for the left wing panels for all the models tested were lower in comparison with the right wing panel. As might be expected under these conditions, the left wing fluttered before the right wing for all cases. Therefore, the data presented in figures 4 and 5 and in table II are for the left wing panels of the respective models.

Flutter Characteristics

The flutter boundary of models 1a and 1b is presented in figure 5 in terms of V_e/V_R plotted against M_e. Also, for comparison purposes the data for the wing plan forms which are designated as the 245 and 445 wings in reference 1 are plotted in figure 5. The 245 and 445 wings had the quarter-chord line swept back 45°, a taper ratio of 0.6, and aspect ratios of 2.4 and 4.0, respectively.

In the subsonic speed range the results of the present tests compare well with the data of reference 1 inasmuch as the V_e/V_R curve for models

1a and 1b (A = 3.0) falls approximately midway between the flutter boundaries of the wings having aspect ratios of 2.4 and 4. However, above $M_e = 1.0$, the flutter boundary for the modified configuration does not fall in line with the results of reference 1. For the present tests there is a rapid increase in V_e/V_R near $M_e = 1.0$ up to a value of $\frac{V_e}{V_R} = 1.4$, after which the value of V_e/V_R changes only slightly as the Mach number is increased to 1.4. In comparison, the data of reference 1 indicate smooth curves throughout the Mach number range with the slopes of the V_e/V_R curves increasing rapidly with Mach number above $M_e = 1.0$.

In order to obtain a more direct comparison with the wings in reference 1, the model of the basic configuration (model 2a) was tested. The data of the tests of model 2a are plotted in figure 5 and are designated by the square symbols. It appears that modifying the inboard wing sections had little, if any, effect on the flutter-speed ratio except possibly as indicated by the points shown at a Mach number of 1.3.

The data of figure 6 are presented as a ratio of experimental flutter frequency to the calculated reference flutter frequency (ω_e/ω_R plotted against M_e). This plot shows an increase in ω_e/ω_R near $M_e = 1.0$ and the general level of ω_e/ω_R curve in the supersonic range is somewhat higher than the general ω_e/ω_R level in the subsonic range. Such an abrupt change in the flutter frequency is not shown by any of the results of reference 1 and could, perhaps, indicate a change in flutter mode. This characteristic has been verified by some unpublished data on a similar wing plan form with a taper ratio of 0.2. For the 0.2-taper-ratio wing the change in flutter frequency was more pronounced than in the present investigation. However, the 0.2-taper-ratio wing had a markedly different natural frequency spectrum from the wings of the present investigation. The differences in the results obtained for the wings of the present investigation as compared with those of reference 1 (fig. 5) indicate the need for further study of highly tapered wings in the range of aspect ratio from 2.0 to 4.0.

The data for the flow conditions at the start of flutter and the various associated parameters for the data presented in figures 4, 5, and 6 are given in table II.

Effect of Flutter-Boundary Shape

For an airplane flying at a given altitude, the importance of the manner in which the flutter boundary varies with Mach number was discussed

in reference 1. The discussion pointed out that the flutter boundaries which were characterized by a "knee" were more desirable than the boundaries with approximately zero slope. For the present investigation the boundary has a break or knee (fig. 5) near $M_e = 1.0$ but the curve flattens out at the higher Mach numbers. This shape of the boundary is undesirable in that an airplane may clear the knee and yet intersect the flutter boundary at a somewhat higher Mach number.

CONCLUDING REMARKS

Results of flutter tests at transonic speeds of a model of a 45° sweptback-wing configuration, which was modified by changing the leading- and trailing-edge sweep angles over the inboard part of the span, indicated a rather abrupt increase in flutter-speed ratio (ratio of experimental to calculated incompressible flutter speed) near a Mach number of 1.0, after which the flutter-speed ratio changed only slightly as the Mach number was increased to 1.4. Flutter characteristics of the basic configuration having straight leading and trailing edges were similar to those of the modified wing and showed that alteration of the inboard sections had little effect on the flutter-speed ratio. Also, the need for further study of the flutter characteristics of highly tapered wings in the range of aspect ratios from 2.0 to 4.0 is indicated.

Langley Aeronautical Laboratory,
National Advisory Committee for Aeronautics,
Langley Field, Va., September 11, 1956.

REFERENCES

1. Unangst, John R., and Jones, George W., Jr.: Some Effects of Sweep and Aspect Ratio on the Transonic Flutter Characteristics of a Series of Thin Cantilever Wings Having a Taper Ratio of 0.6. NACA RM L55I13a, 1955.

2. Bursnall, William J.: Initial Flutter Tests in the Langley Transonic Blowdown Tunnel and Comparison With Free-Flight Flutter Results. NACA RM L52K14, 1953.

3. Barmby, J. G., Cunningham, H. J., and Garrick, I. E.: Study of Effects of Sweep on the Flutter of Cantilever Wings. NACA Rep. 1014, 1951. (Supersedes NACA TN 2121.)

TABLE I.- MODEL PARAMETERS

[All values at $\eta = 0.05$ are extrapolated]

η	x_α	a	r_α^2	m, slugs/ft	b/b_r	EI, lb-in.^{2}	GJ, lb-in.^{2}
Model 1a							
0.05	0.005	0.255	-0.127	0.00980	0.951	----	----
.15	-.001	.250	-.120	.00823	.880	----	----
.25	-.008	.242	-.115	.00699	.806	----	----
.35	-.014	.240	-.108	.00597	.732	3230	1790
.45	-.020	.240	-.103	.00502	.659	2240	1010
.55	-.022	.240	-.097	.00413	.585	1560	645
.65	-.010	.250	-.091	.00341	.514	1120	440
.75	.011	.265	-.085	.00277	.459	820	320
.85	.071	.298	-.079	.00217	.408	560	240
.95	.064	.355	-.074	.00161	.355	330	190
Model 1b							
0.35	-------	-----	------	-------	-----	3170	1370
.45	-------	-----	------	-------	-----	2330	930
.55	-------	-----	------	-------	-----	1670	620
.65	-------	-----	------	-------	-----	1160	420
.75	-------	-----	------	-------	-----	780	290
.85	-------	-----	------	-------	-----	520	210
.95	-------	-----	------	-------	-----	340	160
Model 2a							
0.05	-0.138	0.018	0.267	0.00768	0.970	----	----
.15	-.129	.011	.265	.00698	.908	----	----
.25	-.120	.005	.263	.00628	.843	----	----
.35	-.110	-.003	.260	.00557	.785	2770	1380
.45	-.098	-.012	.253	.00487	.723	2050	830
.55	-.084	-.023	.250	.00417	.662	1500	560
.65	-.066	-.039	.256	.00347	.602	1080	395
.75	-.043	-.056	.267	.00281	.540	760	285
.85	-.015	-.076	.282	.00226	.478	530	200
.95	.025	-.097	.292	.00188	.417	380	130

[redacted]

TABLE II.- EXPERIMENTAL AND ANALYTICAL RESULTS

[μ is the value at $\eta = 0.75$ station]

ρ_e, slugs/cu ft	q_e, lb/sq in.	ω_e, radians/sec	V_e, ft/sec	M_e	ω_R, radians/sec	V_R, ft/sec	V_e/V_R	ω_e/ω_R	μ	$\frac{V_e}{b_r\omega_e\sqrt{\mu}}$
Model 1a										
0.0054	11.74	1696	779	0.709	1573	711	1.095	1.078	9.58	0.385
.0052	14.17	1678	831	.779	1569	720	1.155	1.070	9.96	.403
.0043	12.21	1548	902	.855	1546	769	1.173	1.001	12.04	.398
.0036	11.58	1483	956	.929	1525	820	1.155	.973	14.38	.386
.0059	19.39	1903	971	1.014	1584	693	1.400	1.201	8.78	.502
.0051	17.84	1778	1006	1.028	1566	724	1.389	1.136	10.15	.483
.0051	18.46	1828	1016	1.051	1566	724	1.403	1.167	10.15	.489
.0046	18.07	1759	1063	1.082	1554	751	1.415	1.132	11.25	.485
.0035	17.21	1635	1182	1.197	1522	828	1.426	1.074	14.79	.470
.0035	17.09	1690	1190	1.210	1522	823	1.437	1.110	14.79	.479
.0035	20.09	1759	1278	1.367	1522	328	1.544	1.156	14.79	.496
Model 1b										
0.0079	12.73	1595	680	0.648	1627	644	1.066	1.044	6.55	0.407
.0070	12.82	1590	724	.715	1607	622	1.094	.990	7.40	.407
.0057	12.67	1571	798	.791	1580	700	1.041	.994	9.08	.405
.0051	12.43	1529	837	.846	1566	725	1.155	.976	10.15	.402
.0037	11.16	1520	934	.900	1529	812	1.151	.971	13.98	.383
.0035	11.76	1395	982	.956	1522	828	1.186	.917	14.79	.391
.0034	13.02	1520	1044	1.012	1517	836	1.248	1.002	15.21	.410
.0044	16.60	1696	1045	1.048	1549	763	1.420	1.095	11.76	.467
.0037	14.75	1560	1066	1.070	1529	812	1.313	1.021	13.98	.437
.0042	18.30	1734	1124	1.169	1544	776	1.448	1.124	12.31	.491
.0033	17.21	1623	1222	1.297	1513	844	1.447	1.073	15.77	.471
.0033	18.52	1728	1262	1.316	1513	844	1.495	1.142	15.77	.477
.0032	17.47	1650	1279	1.325	1508	852	1.500	1.094	16.16	.487
Model 2a										
0.0067	11.96	1627	716	0.680	1474	610	1.173	1.103	7.58	0.499
.0041	10.81	1533	872	.822	1441	717	1.215	1.064	12.38	.475
.0034	10.36	1420	931	.906	1431	774	1.202	.993	14.93	.463
.0041	14.37	1546	1008	1.013	1441	717	1.406	1.073	12.38	.546
.0032	17.66	1703	1237	1.288	1428	799	1.573	1.193	15.87	.608
.0034	17.63	1684	1238	1.316	1431	774	1.600	1.176	14.93	.614

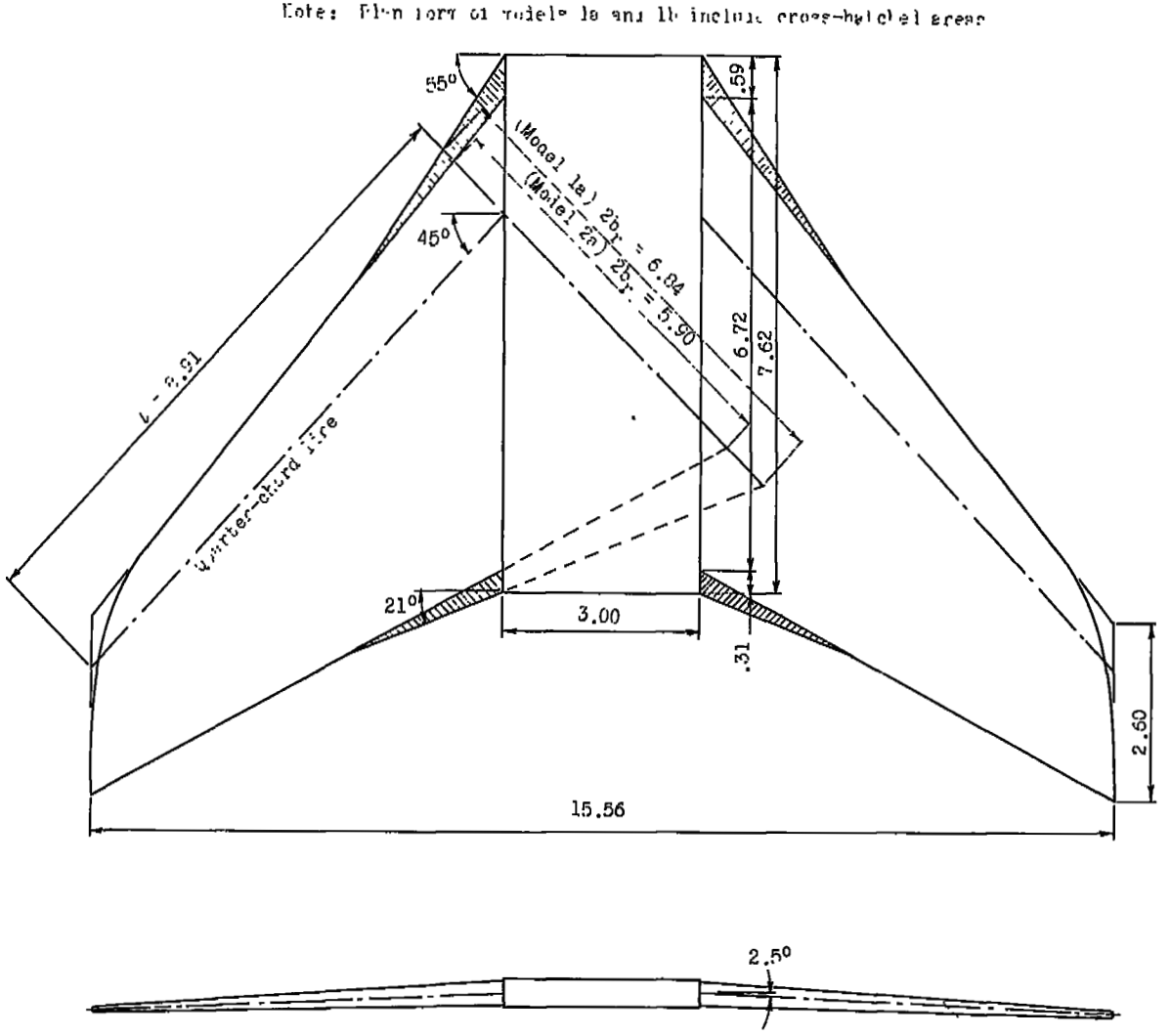

Figure 1.- Details and dimensions of models tested. (All dimensions are in inches unless otherwise stated.)

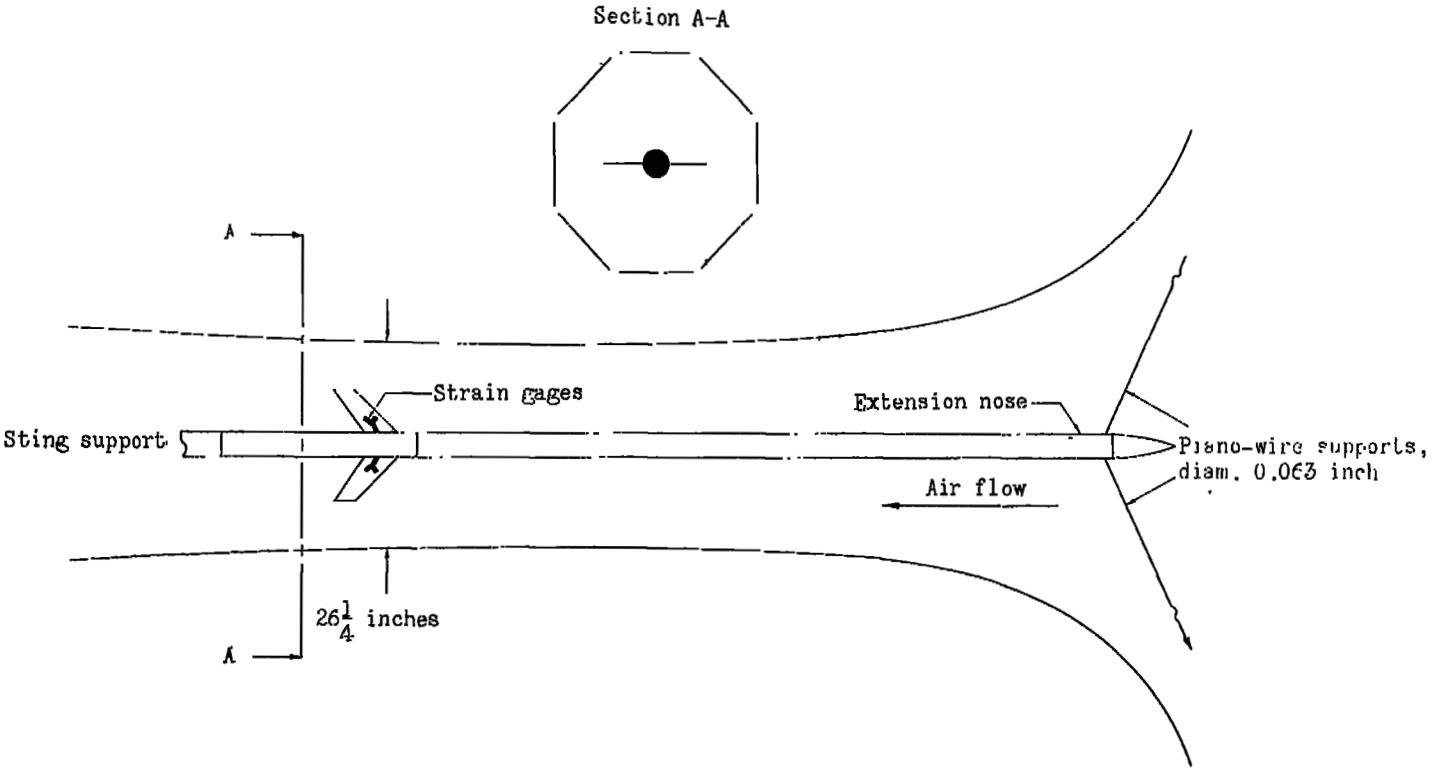

Figure 2.- Plan view of Langley transonic blowdown tunnel with flutter model installed.

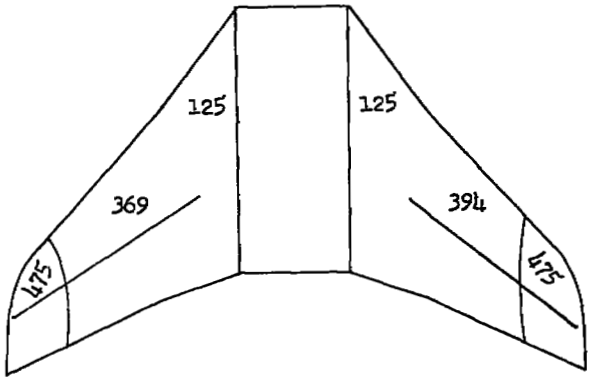

(a) Model 1a.

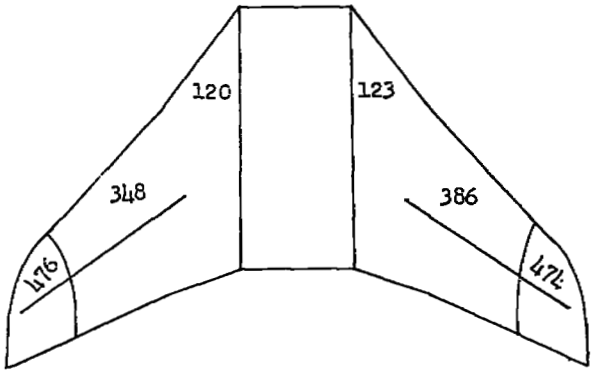

(b) Model 1b.

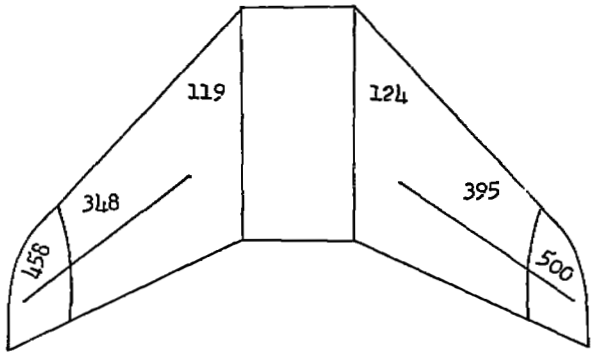

(c) Model 2a.

Figure 3.- Measured model frequencies and node lines. Frequencies are in cycles per second.

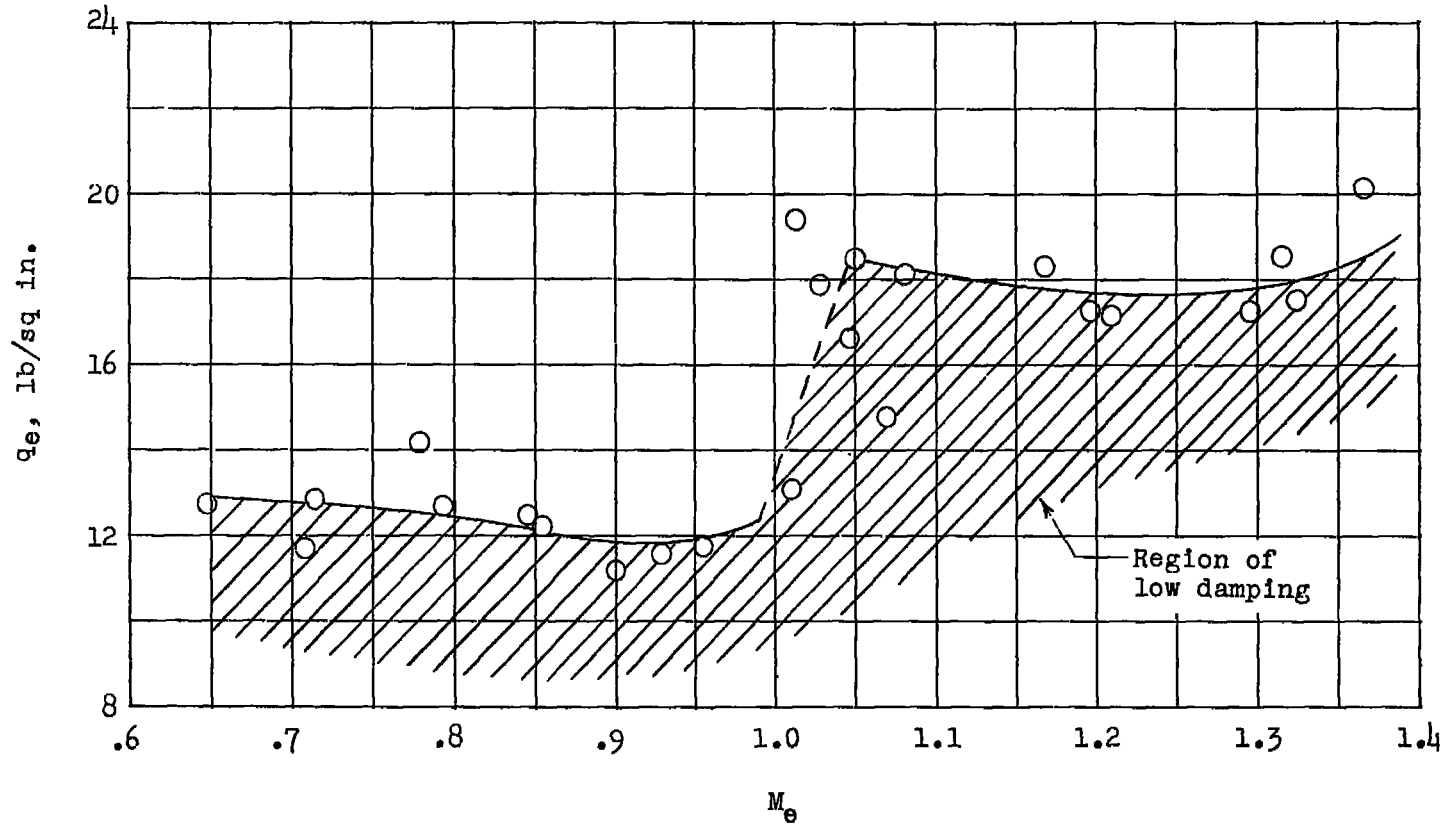

Figure 4.- Variation of experimental flutter dynamic pressure with Mach number. Models 1a and 1b.

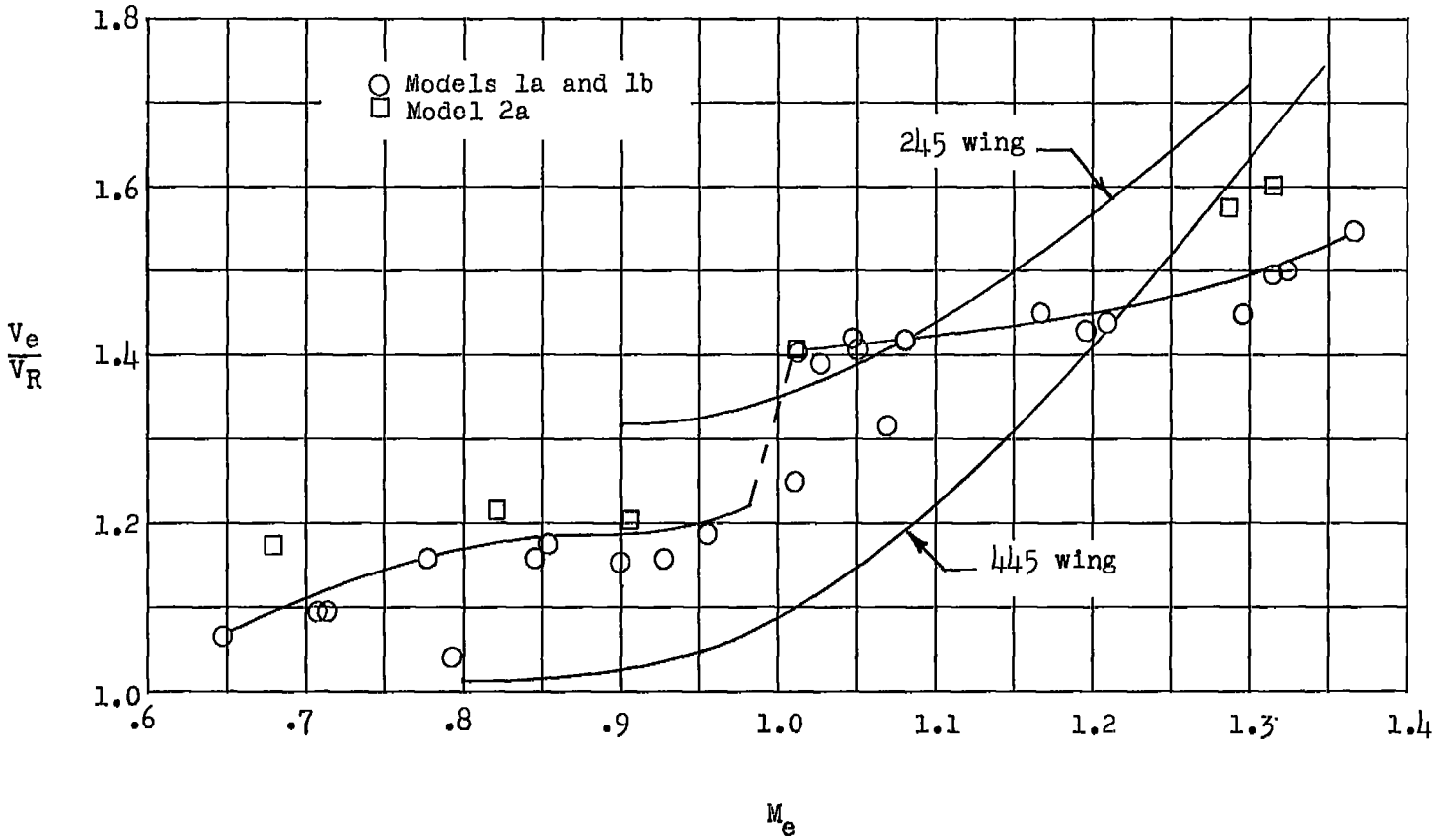

Figure 5.- Variation of flutter-speed ratio with Mach number. Models 1a, 1b, and 2a.

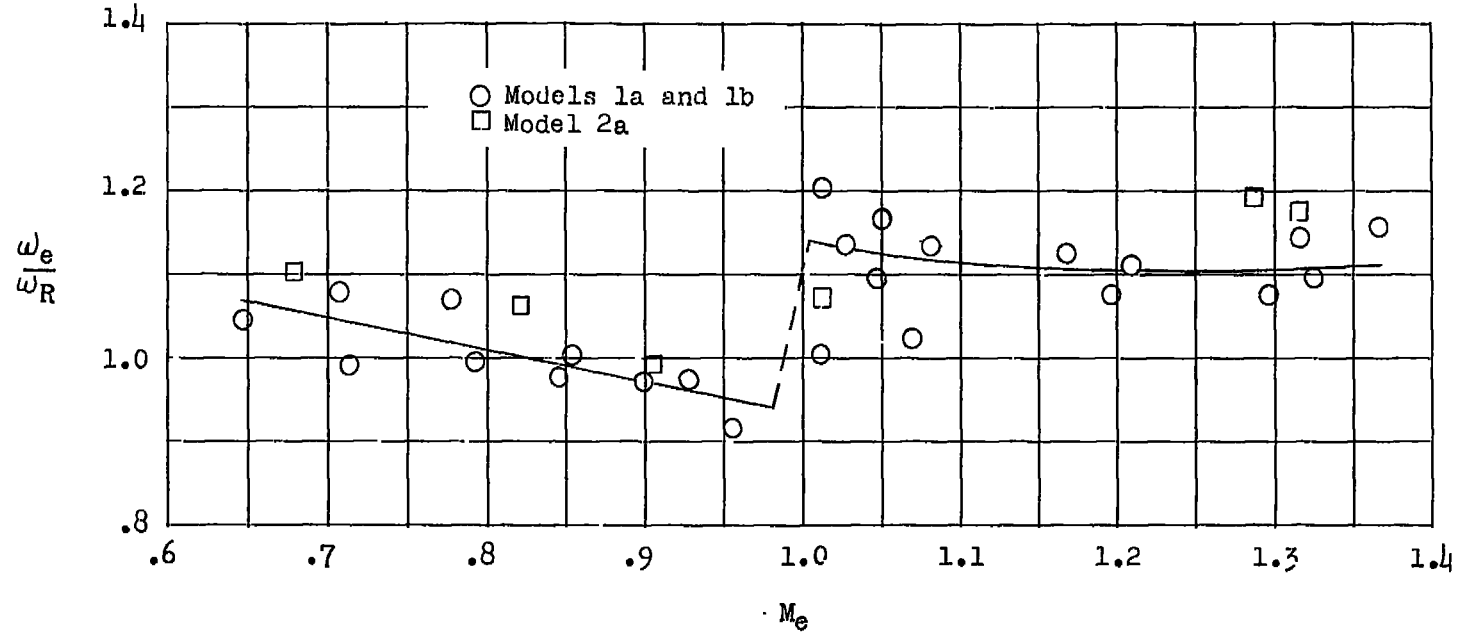

Figure 6.- Variation of flutter frequency ratio with Mach number. Models 1a, 1b, and 2a.